Spectral Self-Interference Fluorescence Microscopy for Subcellular Imaging

Mehmet Doğan, *Student Member, IEEE*, Ayça Yalçın, *Student Member, IEEE*, Sumita Jain, Marcia B. Goldberg, Anna K. Swan, *Senior Member, IEEE*, M. Selim Ünlü, *Fellow, IEEE*, and Bennett B. Goldberg

(Invited Paper)

***Abstract*—Spectral self-interference fluorescence microscopy (SSFM) has been recently developed to determine the axial position of fluorescent emitters placed on reflecting dielectric structures. In this paper, we review SSFM with emphasis on its axial localization capabilities. We show that there is a tradeoff between the numerical aperture (NA) of the microscopy system and the axial localization fidelity. To use high-NA objectives for better lateral resolution, we describe and demonstrate a high-NA 4Pi microscopy system that performs spectral self-interference microscopy for axial localization of less than 2 nm. We demonstrate axial localization by using artificial samples. We also probe the membrane topography of a *Shigella flexneri* bacterium, several micrometers away from a solid support.**

***Index Terms*—Fluorescence microscopy, localization, self-interference, subcellular imaging.**

I. Introduction

FLUORESCENCE microscopy is an indispensable tool in modern biological research. It provides a high-contrast and high-sensitivity imaging modality by employing fluorescent markers capable of attaching to specific biochemical targets. Recent advances in fluorophore chemistry have further enabled a wide variety of fluorescent markers to tag many different types of biomolecules to be used in both structural and functional studies of cells.

Despite its advantages, fluorescence microscopy is limited by diffraction [1]. While the resolution of fluorescence microscopes used in cell biology is typically hundreds of nanometers, most subcellular structures are much smaller and require resolution of tens of nanometers.

Manuscript received September 21, 2007; revised October 19, 2007. This work was supported in part by the U.S. National Science Foundation under Grant DBI 0138425 and Award EEC-9987821 of the Engineering Research Centers Program, in part by the Air Force Office of Scientific Research under Grant MURI F-49620-03-1-0379, and in part by the National Institutes of Health, National Institute of Biomedical Imaging and Bio Engineering under Grant 5R01 EB00 756-03.

M. Doğan and B. B. Goldberg are with the Physics Department, Boston University, Boston, MA 02215 USA (e-mail: mdogan@bu.edu; goldberg@bu.edu).

A. Yalçın, A. K. Swan, and M. S. Ünlü are with the Electrical and Computer Engineering Department, Boston University, Boston, MA 02215 USA (e-mail: ayca@bu.edu; swan@bu.edu; selim@bu.edu).

M. B. Goldberg is with the Department of Medicine, Massachusetts General Hospital and Harvard Medical School, Division of Infectious Diseases, Cambridge, MA 02139 USA (e-mail: mgoldberg1@partners.org).

S. Jain was with the Department of Medicine, Massachusetts General Hospital and Harvard Medical School, Division of Infectious Diseases, Cambridge, MA 02139 USA. She is now with the Department of Periodontics, University of Washington, Seattle, WA 98195 USA (e-mail: sumita@u.washington.edu).

Color versions of one or more of the figures in this paper are available online at http://ieeexplore.ieee.org.

Digital Object Identifier 10.1109/JSTQE.2008.912901

Within the last few decades, an increasing number of novel fluorescent imaging techniques have been introduced to circumvent the fundamental diffraction limit. One of these techniques is 4Pi confocal fluorescence microscopy, which is based on coherent illumination of fluorophores and collection of emission by using two opposing objectives [2]. Coherent use of two objectives in 4Pi microscopy increases the collection angle and improves the axial resolution by five- to seven-fold as compared to standard fluorescence confocal microscopes [3].

Nonlinear effects in fluorescence have also been exploited to overcome the diffraction barrier in fluorescence microscopy. In stimulated emission depletion (STED) microscopy, fluorescence is quenched by stimulated emission of excited fluorophores before they fluoresce [4], [5]. Depletion in an annular region around a central spot reduces the fluorescence emission to arbitrarily small volumes, and in theory, diffraction-unlimited resolution is possible. Nonlinear structured illumination wide-field microscopy has also shown 2-D resolution of less than 50 nm as long as samples are bright and photostable providing high SNR [6].

While a tremendous effort is being conducted toward improving the 3-D resolution of far-field fluorescence microscopes, localization of fluorescent structures with high accuracy is also of ample interest. Localization refers to how well the position of the known object can be determined, and should be distinguished from resolution, which refers to the ability of distinguishing two nearby objects. Usually, high SNR and *a priori* knowledge about the object help increase the fidelity of the position determination process. Examples include localization of single molecules to explain the way molecular motors like myosin V and kinesin move along microtubules in a cell [7], [8]. Recently, two new techniques, stochastic optical reconstruction microscopy (STORM) [9] and photoactivated localization microscopy (PALM) [10], have been introduced that exploit parallel localization of sparse emitters by estimating the center of the emission point spread function of the emitters. In principle, both techniques rely on the constraint that the fluorescence emission originates from single molecules during the integration time of the detection system and the separation between the molecules is larger than the resolution limit of the system.

Fluorescence emission can also be localized in the axial dimension if the fluorescent objects exhibit sparse axial distributions. Even though the axial resolution is typically limited to hundreds of nanometers, nanometer-scale localization can be achieved by utilizing the interference in both the excitation and emission channels. It has been known for many years

that fluorescence emission is modified by nearby dielectric or metal surfaces [11]–[13]. In the 1970s, Drexhage measured the fluorescence lifetime of organic dyes placed on stepped lipid bilayers to show the dependence of lifetime to the distance from a reflector [14]. Later, Fromherz and coworkers developed a fluorescent localization technique, fluorescence interference contrast (FLIC) microscopy, based on the change in the total emission intensity as a function of distance from a nearby reflecting substrate [15]–[17]. In FLIC microscopy, the fluorescently labeled object is placed on top of a Si substrate with a SiO_2 spacer in between. The optical thickness of the spacer layer is less than one wavelength to avoid smearing of the emission intensity due to differences in the interference of different wavelengths and angular components. Axial position information is extracted from the total emission intensity, and therefore, calibration of the position as a function of intensity is required. The samples under investigation also have to be labeled uniformly; otherwise, any change in the density of fluorophores within the object results in a change in intensity, and can be misinterpreted as a position shift.

Another fluorescent microscopy technique that utilizes the interference for axial localization is the spectral self-interference fluorescence microscopy (SSFM) [18]. Here, instead of monitoring the modified total emission intensity, spectral oscillations in the fluorescent emission induced by the presence of a reflecting surface are used to identify the position of emitters with respect to the reflector.

In this paper, we first review the SSFM technique in view of its localization capabilities. We show that high-numerical-aperture (NA) objectives are not feasible in SSFM on flat substrates, as the fringe visibility of spectral oscillations decreases with increasing NA, and consequently, the localization precision is degraded. In Section II, we describe a hybrid fluorescence microscopy system, 4Pi-spectral self-interference microscope (4Pi-SSFM), which is capable of nanometer-scale axial localization while using high-NA objectives. With the microscope, we demonstrate the localization of fluorescent emitters tagged to the outer membrane of *Shigella flexneri*, a gram-negative bacterium.

II. SSFM on Planar Surfaces

Emitters placed in cavities or near reflecting structures exhibit modified spontaneous emission rates and intensities [19]–[21]. Wavelength dependence of this modification changes the spectral shape of the emission. The SSFM utilizes this kind of spectral modification to reveal the position of fluorescent emitters. In SSFM, the objects under investigation are labeled with fluorescent emitters and are fixed above a reflecting Si surface with SiO_2 in between as a spacer. Unlike in FLIC microscopy, the spacer thickness is much larger compared to the wavelength, typically ten wavelengths. Instead of utilizing the emission intensity variations with changing fluorophore position, the SSFM uses spectral intensity oscillations as a function of axial position of the emitter from the reflector. Modification of the spectrum can be viewed as a result of the interference of the two available pathways from the emitter to the detector, the direct optical path and the reflected path from the highly reflecting Si surface. Depending on the axial position, certain wavelength components of the spectrum that experience constructive interference are enhanced while some other portions undergo destructive interference, diminishing the signal. Thus, the optical distance between the reflecting Si and the molecule precisely dictates how these oscillations form within the spectral envelope of the fluorophores. Fig. 1(a) shows the spectral oscillations in the emission spectrum of Alexa Fluor 647 (AF647) fluorophores immobilized on two levels of SiO_2 spacer on top of Si, as illustrated in Fig. 1(b).

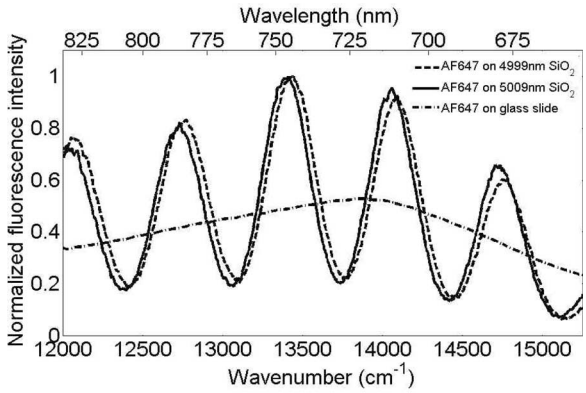

(a)

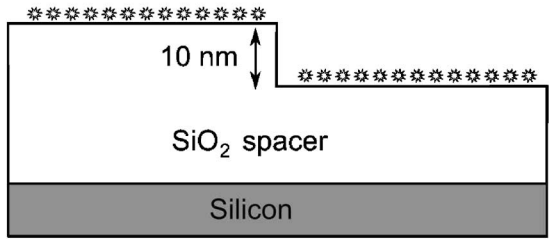

(b)

Fig. 1. (a) Emission spectra of Alexa Fluor 647 (AF647) on top of a Si–SiO_2 substrate. Spectra exhibit spectral interference fringes that are shifted for two different thicknesses of the SiO_2 layer. Spectral envelope of AF647 measured on top of a glass slide is shown for comparison (no interference). (b) Schematic of the Si–SiO_2 substrate. Nominal thickness of the oxide layer is 5 μm; the step is 10 nm (not to scale).

An SSFM system consists of a continuous wave laser as the excitation source, an epifluorescence microscope, and a spectroscopy system. In the previous studies [18], [22], [23] and in this paper, an upright microscope and a micro-Raman spectrometer were used. The excitation beam was expanded, coupled to the microscope objective through the side port of the microscope and focused onto the sample. The emitted signal was collected with the same objective, and any residual excitation laser light was filtered using a notch filter. The signal was then coupled to the spectrometer for spectral acquisition. A grating of 1800 grooves per millimeter was used with a spectral resolution of $2\,\mathrm{cm}^{-1}$ at 500 nm. The spectral signal was recorded by using a thermoelectrically cooled charge coupled device (CCD). The substrates shown in Fig. 1(b) were several millimeter

square pieces of Si wafers with 5-μm-thick SiO_2 layers grown by plasma-enhanced chemical vapor deposition (PECVD).

Using a classical electromagnetic model that incorporates reflections from dielectric boundaries in the substrates, oscillations in the spectra can be analyzed to reveal axial position. In the early studies of SSFM [18], a simple ray optics model was used by employing far-field approximations of a radiating dipole. Later, it was shown that this simple model converges to the results obtained by a rigorous Green's function approach in the far field [23].

In the emission model, each fluorophore is modeled as an oscillating dipole emitter with a random orientation over a Si–SiO_2 substrate. Each dipole emitter is assumed to be incoherent with the other radiating dipoles within the excitation volume as fluorescence is a spontaneous process. The total intensity due to an arbitrarily oriented single dipole is calculated over the lens aperture by including the polarization of the radiation field and the generalized Fresnel reflection coefficients. Finally, the total intensity collected by the objective lens is averaged over all possible dipole orientations. As a result, the total emission of random dipoles collected with an objective of maximum collection angle $\theta_{em}^{\max}$is expressed as

$$I_{\text{total}} = \int_{\theta=0}^{\pi/2} \int_{\varphi=0}^{\pi} \int_{\theta_{em}=0}^{\theta_{em}^{\max}} I(\theta, \varphi, \theta_{em}) \sin\theta_{em}\, d\theta_{em}\, d\varphi\, d\theta \tag{1}$$

where θ is the polar tilt of the dipole, φ is the azimuthal angle of the observation direction, and $I(\theta, \varphi, \theta_{em})$is the emission intensity of a single dipole. In SSFM, the modifications to the spectral shape are of interest rather than the absolute intensity. Therefore, any constants in the expressions are dropped, and only the angular dependence of the radiation is considered. In fact, the radiation intensity of an oscillating dipole is inversely proportional to the fourth power of the wavelength. Nevertheless, this dependence is already embedded in the spectral envelope of the fluorophore and we do not include it in our emission model that only predicts the oscillatory component of the emission due to reflecting interfaces, and therefore, the localized position of the emitter.

The spectral self-interference data is composed of an oscillatory component generated by the presence of nearby reflecting surfaces and the spectral envelope of the fluorophores. The oscillatory component is a function of system parameters such as the refractive indices of Si and SiO_2, NA of the collection system, orientation of the fluorophore dipole moments, and the axial position of the emitter with respect to the reflector. If the dipoles exhibit a well-defined orientation, in principle, their orientation can be extracted from the spectral data. For the samples used in this study, the dipoles are assumed to be randomly oriented, and only the axial position is used as the fitting parameter for the oscillatory component. The envelope of the spectrum is independent of the system parameters and is free from spectral variations comparable to those in the oscillatory component. In general, it can be described by a polynomial of low order. We constrain the order of the polynomial in the envelope function in the fitting procedure, since we want to avoid any competition between the higher orders of the envelope and the oscillatory components due to interference. Initially, an axial position value is estimated, and the oscillatory component is generated using our forward model. As a second step, the raw data is divided by the generated function. The division results in a function representing the spectral envelope of the emission. An incorrect estimation yields an envelope function that is not decoupled from the oscillations, and the restricted polynomial fit results in a large error. If the axial position is correct, the resulting envelope function is free from oscillations and can be fit by a low-order polynomial with the lowest least square.

It is crucial to assess the capabilities of the SSFM by analyzing the parameters involved in the technique such as fringe visibility, collection NA, and spectral bandwidth, and their effects on localization. Fringe visibility of the spectral interference data is a critical parameter as the axial position information is encoded in the spectral oscillations. After the spectral envelope is removed from the spectrum, we define spectral fringe visibility as

$$V = \frac{I_{\max} - I_{\min}}{I_{\max} + I_{\min}} \tag{2}$$

where $I_{\max}$ is the maximum and $I_{\min}$ is the minimum of the oscillatory component of the spectral signal within the collection bandwidth. For low NA collection systems, the spectral fringe pattern converges to a sinusoidal function, and the visibility is constant throughout a wide spectral range. However, in general, especially when high-NA objectives are employed, the fringe pattern is not a pure sinusoidal function, and the fringe visibility is wavelength- and bandwidth-dependent.

Fringe visibility primarily depends on the axial distribution of the emitters and the NA of the collection objective. If a fluorescent object has some extension along the optical axis, each axial level contributes to the total spectrum with its corresponding interference fringes slightly shifted with respect to other axial levels, and consequently, the overall spectral signal has lower fringe visibility. Similarly, for each angular component of the radiation, the associated path length difference due to the reflection is a function of the wavelength and the emission angle. We demonstrate this effect by plotting the radiation intensity as a function of angle for three wavenumbers, as shown in Fig. 2(a). For different angles, the wavelength dependence of the radiation is not the same, and each angular component appears to carry different axial position information. As a result, the spectral oscillations are shifted for each angular component. This is illustrated in Fig. 2(b), where normalized intensity versus wave number is plotted for two polar angles, 6.9° and 30°. In principle, if a high enough signal is collected within a precisely controlled narrow angular window using annular pupil filters, axial position can be determined without ambiguity. However, limiting the emission angles to narrow ranges would significantly reduce the collection efficiency and is not practical. In SSFM experiments, objective lenses are employed to gather the emission, and all the angular components are integrated within the collection cone for better signal. Nevertheless, integration of angular components results in loss of fringe visibility. The effect of integration can easily be observed, especially for a high-NA, comparing Figs. 2(b) and 3(b). In Fig. 2(b), only one angular

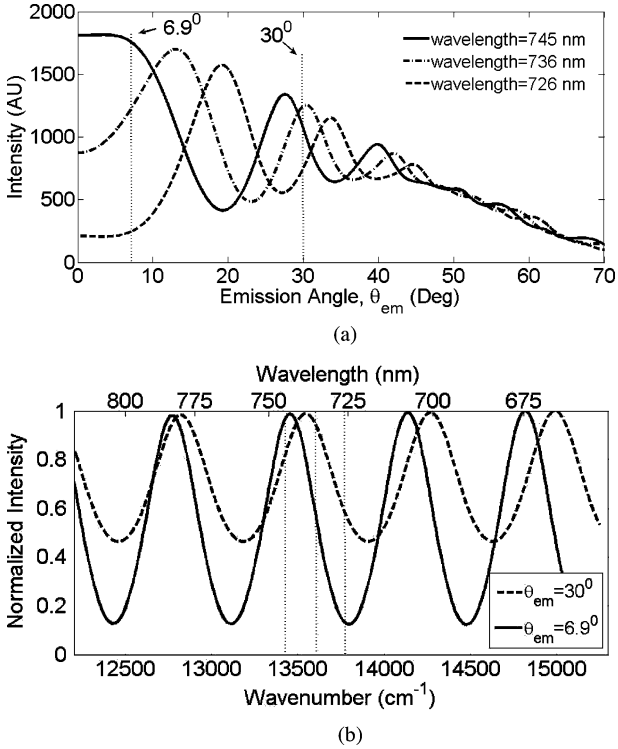

Fig. 2. (a) Calculated fluorescence emission intensity of fluorescent emitters on a Si–SiO_2 substrate for three wavelength values [marked in (b)] as a function of angle measured from the optical axis. The oxide layer thickness was assumed to be 5 μm. Two angles, 6.9° and 30°, that correspond to the maximum collection angles of two NA values, 0.12 and 0.5, are marked on the plot. (b) Calculated spectral fringe patterns for 6.9° and 30°. Three wavelength values, 745, 736, and 726 nm, respectively, are marked on the plot.

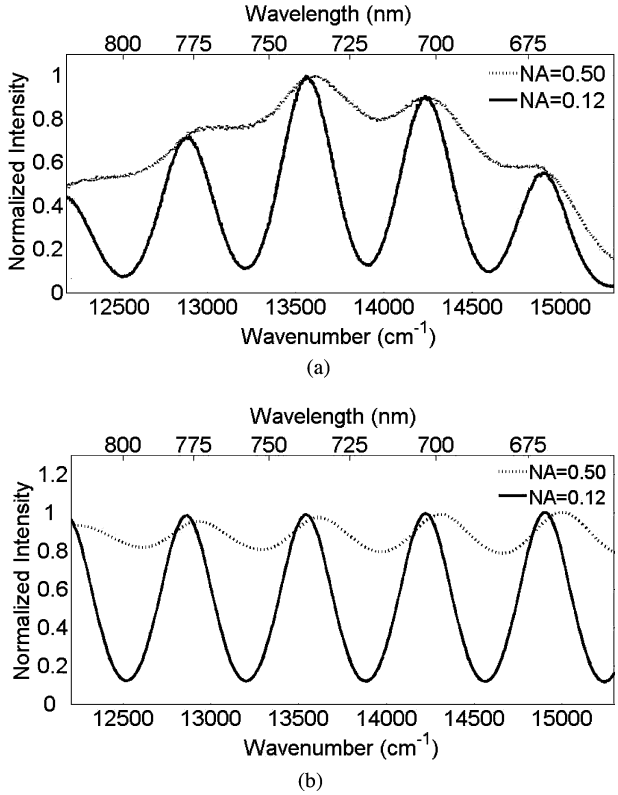

Fig. 3. (a) Measured fluorescence emission from AF647 as a function of wavenumber for two different objectives: NA = 0.5 and NA = 0.12. The fringe visibility decreases with increasing NA. (b) Simulated oscillations as a function of wavenumber for two different objectives: NA = 0.5 and NA = 0.12. The spectral envelope of the emitters is not included in the simulation. Note that the spectral fringe pattern is calculated by integrating the angular emission components up to the maximum collection angle of each objective.

component of intensity is considered, whereas in Fig. 3(b), the emission intensity is integrated up to the maximum collection angle of the corresponding NA to simulate the collection with an objective.

Numerical aperture dependence of fringe visibility is experimentally demonstrated in Fig. 3(a). Spectral data were acquired from AF647 fluorophores immobilized on Si–SiO_2 substrates. Two objectives with NAs of 0.12 and 0.5 were used subsequently to probe the same point on the sample. The collected spectra consist of the spectral envelope of the emitter and oscillatory components. For comparison, simulated spectrum due to a random dipole is also shown in Fig. 3(b), and only the oscillatory component is considered. In the simulation, the oxide thickness was assumed to be 4.967 μm, which is the axial position of the emitters whose spectra are shown in Fig. 3(a). While the fringe visibility is about 0.8 for an NA of 0.12, it is only 0.12 for an NA of 0.5. For a continuous set of NA values, the visibility is shown as a function of the maximum collection angle in Fig. 4, where a drastic drop in fringe visibility for high-NA values is demonstrated.

To characterize how well the fitting would predict the axial position for a given visibility, we simulated the spectral emission data of a monolayer of AF647 on Si–SiO_2 substrates for two different NA values, 0.12 and 0.5. Poisson noise was then added to the synthetic data, and the fitting procedure was applied to

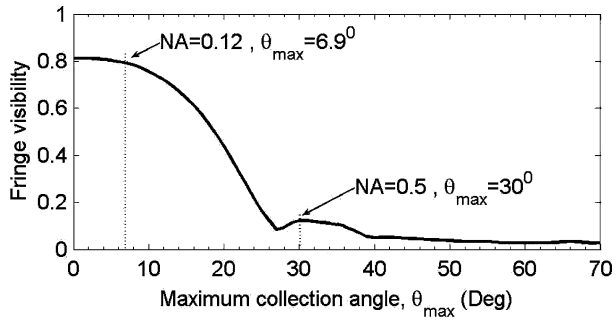

Fig. 4. Spectral fringe visibility as function of maximum collection angle. Two numerical aperture values (0.12 and 0.5) with the corresponding maximum collection angles are marked on the graph. The fringe visibility decreases with increasing NA.

find the axial position. In this Monte Carlo approach, the axial position results from 1000 spectra were plotted in a histogram. A Gaussian fit to the histogram was used to define a full-width at half-maximum (FWHM) to quantify the uncertainty in the fitting procedure. For a maximum signal of 1000 counts and for an NA of 0.12, the FWHM of the estimation was found to be 0.78 nm [Fig. 5(a)]. The uncertainty increased as the SNR dropped with the decreasing signal. For maximum signal counts of 100 and 10, the uncertainties came out to be 2.64 and 8.97 nm,

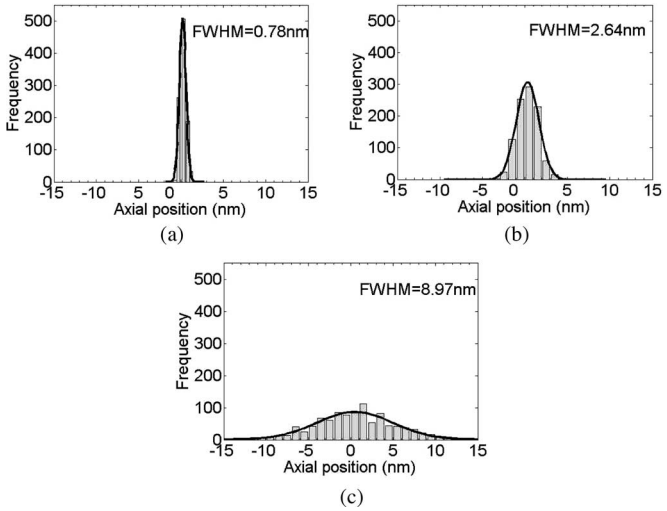

Fig. 5. Histograms of axial position values after the fitting procedure is applied on the synthetic spectral data of AF647 on Si-SiO_2 substrates for maximum signal counts of (a) 1000, (b) 100, and (c) 10. The NA of the objective was assumed to be 0.12; the oxide thickness was taken as 5 μm. In each set, 1000 spectra were fitted. A spectral range of 12 000 to 15 300 cm^{-1} was used in fittings. Horizontal axes represent axial position values in nanometers relative to the 5 μm nominal value. Vertical axes represent the number of occurrences for a given position deviation. A Gaussian fit is plotted on top of the histograms and FWHM values of the fits are shown as a measure of axial uncertainty. The axial uncertainty increases with decreasing signal counts.

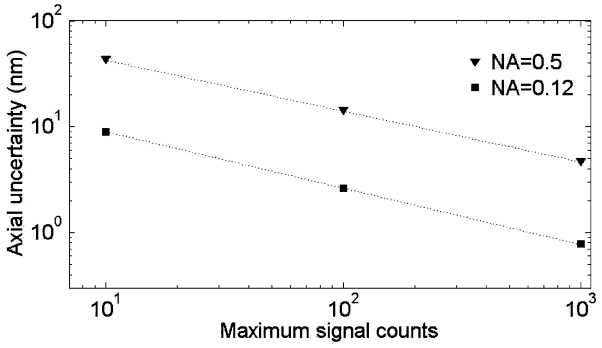

Fig. 6. FWHM values of the fitting histograms defined as axial uncertainty vs. maximum signal counts for two NA values of 0.5 and 0.12.The oxide thickness was taken as 5 μm. The axial uncertainty decreases with increasing signal counts and decreasing NA.

respectively [Fig. 5(b) and (c)]. For an NA of 0.5, due to the reduction in the fringe contrast, the uncertainty in the axial position estimation was 4.7 nm even for 1000 counts. For signal counts lower than 100, the estimation uncertainty was worse than 10 nm. We compare the uncertainties in axial localization obtained for two numerical aperture values in Fig. 6.

In order to assess how the width of the emission spectrum affects the localization, we simulated the spectral emission pattern of emitters on top of a Si–SiO_2 substrate with Poisson noise added to each spectrum. For an assumed oxide thickness of 5 μm, an NA of 0.12 and maximum signal counts of 1000, we generated axial position histograms for a set of changing spectral windows centered on the emission peak of the AF647 fluorophore to determine the uncertainty in the axial localization (Fig. 7). We have found that the uncertainty in localization

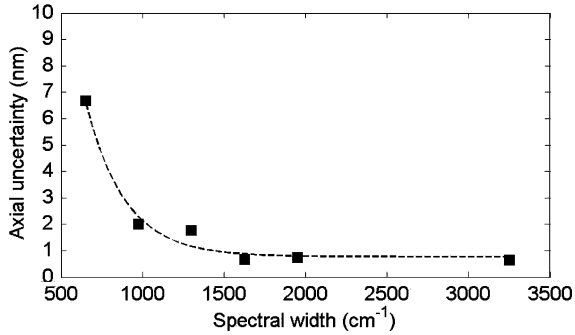

Fig. 7. Axial localization uncertainty determined by the FWHM values of the fitting histograms as a function of spectral width of the data used in the fittings. NA of the objective is assumed to be 0.12; oxide thickness is taken as 5 μm in the simulations. The axial uncertainty decreases with increasing width of the emitters.

increases more drastically for width values narrower than about 1300 cm^{-1}, which corresponds to approximately two periods of the spectral oscillations for a 5 μm oxide thickness. For wider spectral ranges, the uncertainty is found to be almost constant and below 1 nm. For a spectral width of 650 cm^{-1}, the uncertainty is approximately 7 nm. At this width, even if the spectra are simulated with ten-fold higher signal counts, the uncertainty does not improve significantly and is approximately 6 nm. In this technique, rather than the peak emission wavelength or the absolute width of the fluorophores, the number of spectral fringes in the emission is critical. Thus, bright fluorescent sources with wide emission spectra that ensures sufficient number of fringes for a given spacer thickness are desirable for better performance of spectral self-interference microscopes.

Standard spectral self-interference microscopy using planar reflecting substrates, like all other localization methods, is bound by the diffraction limit [24]. However, it is a useful technique to localize axially sparse layer-like objects. By estimating the axial position of fluorescent emitters attached to DNA molecules, the conformation of DNA has been studied on flat substrates [22]. Nevertheless, there is a tradeoff between the axial localization precision and the NA. Since lateral resolution scales with the NA, high-lateral resolution cannot be achieved with standard SSFM systems while estimating the axial position with nanometer precision. Low collection efficiency is another drawback if low NA objectives are employed. In the previous SSFM experiments [18], [22], [23], samples were laterally uniform and high-lateral resolution was not crucial. Thus, high resolution was sacrificed to axial precision by using 0.12 NA objectives. However, in order to probe laterally confined objects while benefiting from axial localization, a different configuration is required.

III. 4PI-SSFM

Despite the capability for high-precision axial position determination, SSFM systems utilizing reflecting planar substrates have relatively poor lateral resolution, as low NA objectives are used to ensure sufficient spectral fringe visibility.

Here, we propose a solution by introducing a second objective instead of a reflecting surface and collecting the emission in both forward and backward axial directions with two identical

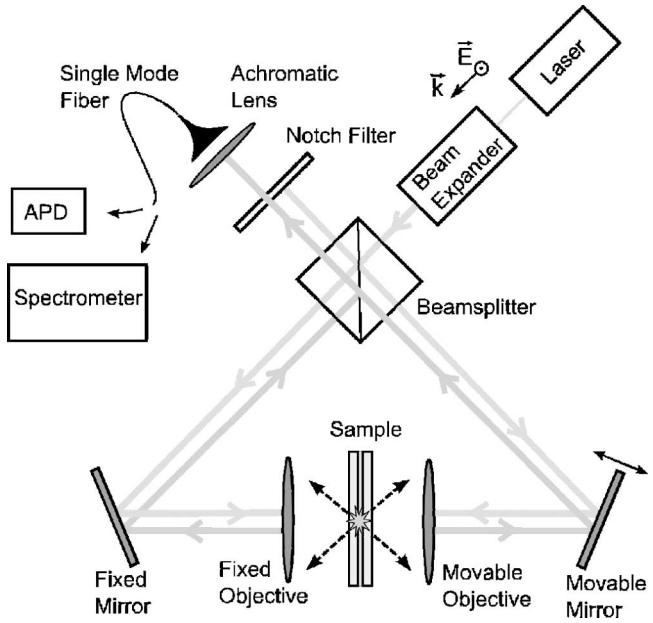

Fig. 8. Schematic of the 4Pi-SSFM. The microscope consists of a triangular interference path, laser source with an expander, and a confocal collection system. Signal can either be coupled to an avalanche photodiode (APD) or a spectroscopy system using the single mode fiber.

objectives. The emission in two opposing directions is combined using a beam splitter to interfere the two collection pathways. This configuration is similar to the 4Pi confocal fluorescence microscopy introduced by Hell [2]. For this reason, we name this new modality of the self-interference microscopy as 4Pi-SSFM. It differs from conventional 4Pi microscopes in that, instead of performing a 3-D confocal scan of the object, axial position determination is done through the spectral emission properties. Experimentally, the phase delay between the two pathways is achieved in the infinity-corrected path beyond the objectives such that all angular components experience the same delay, unlike the angle-dependent phase delay in standard SSFM using planar reflecting surfaces. Due to the symmetric collection, high-NA objectives can be used in 4Pi-SSFM to increase the lateral resolution without losing the fringe visibility.

Fig. 8 shows the schematic of a 4Pi-SSFM system used in the experiments explained later. The system is based on a 4Pi type C confocal microscope [2]. The central interferometer section of the system is composed of a nonpolarizing cube beam splitter, two mirrors, and two matched 1.4 NA oil immersion objectives. While one objective is fixed, the other objective is driven by a piezoelectric stage in a closed-loop operation with nanometer precision. The sample is mounted between the two objectives on an additional piezo stage.

The path length difference between the two arms is adjusted and controlled by one of the mirrors mounted on a piezoelectric controller. Prior to the experiments, the path length difference is adjusted such that there is sufficient number of modulations in the emission spectrum. This difference in the path lengths has similar phase delay functionality to the SiO_2 spacer in a standard reflection mode SSFM system. During spectral measurements, the path length difference is kept at a fixed value.

In conventional 4Pi microscopy, two-photon excitation has been utilized in order to minimize the side lobes of the axial point spread function (PSF) of the microscope. In SSFM, axial localization of layer-like sparse samples is of interest, and the axial extent of the PSF is not as critical. Thus, the excitation source in our experiments is an optically pumped semiconductor continuous wave laser operating at 488 nm. The laser beam is linearly polarized in the direction perpendicular to the triangular cavity formed by the beam splitter and the two mirrors. A beam expander is used to increase the diameter of the excitation laser beam so that the beam fills the back aperture of the objectives.

After the two pathways are combined at the beam splitter, any residual laser signal is removed by using a holographic notch filter operating at 488 nm. The signal is focused to a single-mode fiber using an achromatic lens with a focal length of 30 mm. The fiber core acts as a confocal pinhole with a 4.2 μm mode field diameter and an effective NA of 0.074 at 488 nm.

Once the signal is coupled into the single-mode fiber, the fiber is either connected to the entrance port of an avalanche photodiode (APD) for axial or 3-D confocal scanning of the object, or a spectrometer system for axial localization. The spectroscopy system consists of an $f/4$ spectrometer and a CCD camera with a spectral resolution of 45 pm. We have used the APD mode to adjust and evaluate the axial overlap of the two objectives by scanning the sample axially and to position the specimen to the common foci of the objectives afterwards for spectral measurements.

In 4Pi microscopes, it is critical to colocalize the foci of the two objectives. Prior to the operation of the microscope, foci of the two objectives are matched within several nanometers by moving the piezo-controlled objective in a closed loop. The lateral overlap is ensured through visualization of the interference of the clockwise and counterclockwise traveling beams at the exit port of the beam splitter. A CCD camera and a flip mirror are used to view the interference (not shown in Fig. 8). The axial overlap is first coarsely monitored through the size of the outcoming laser beams that travel through the two objectives, and then, finely adjusted by scanning the sample within the common focus. When the axial response of the fluorescence collected by the movable objective matches with the axial response of the signal through the fixed objective, the foci are axially colocalized.

The axial position of fluorescent monolayers is determined by following the same algorithm that was used for standard SSFM. In fact, the emission model is much simpler in 4Pi-SSFM as there are no reflections involved. Simply, the emission is considered to be isotropic due to the random orientations of the dipoles, and only axial phase relations between the two collection paths are included.

To demonstrate the axial localization capabilities of the 4Pi-SSFM system, we fabricated a ridge pattern with 20 nm deep and 5-μm-wide stripes on a glass microscope cover slip. The stripes were etched using buffered oxide etch. The surface of the coverslip was then amine functionalized by applying 5% 3-aminopropyltriethoxysilane (APTES) in acetone for 2 min. Carboxyl modified Alexa Fluor 488 dye with an absorption maximum of 495 nm and an emission maximum of 519 nm was used

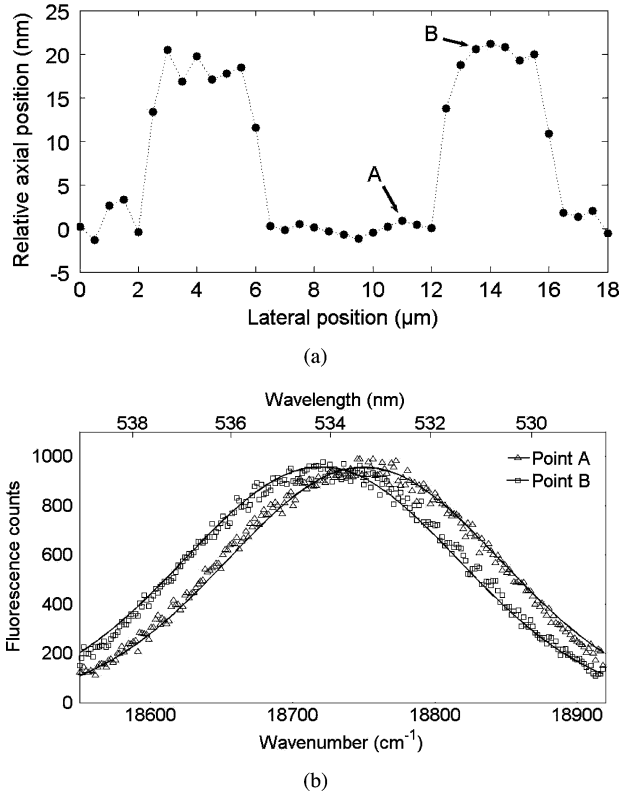

Fig. 9. (a) Axial position values measured by 4Pi-SSFM versus lateral scan direction. 20 nm ridges are recovered from the spectral data. (b) Limited spectral window shows the shift in the spectral fringes between the spectra from two points labeled as A and B in (a).

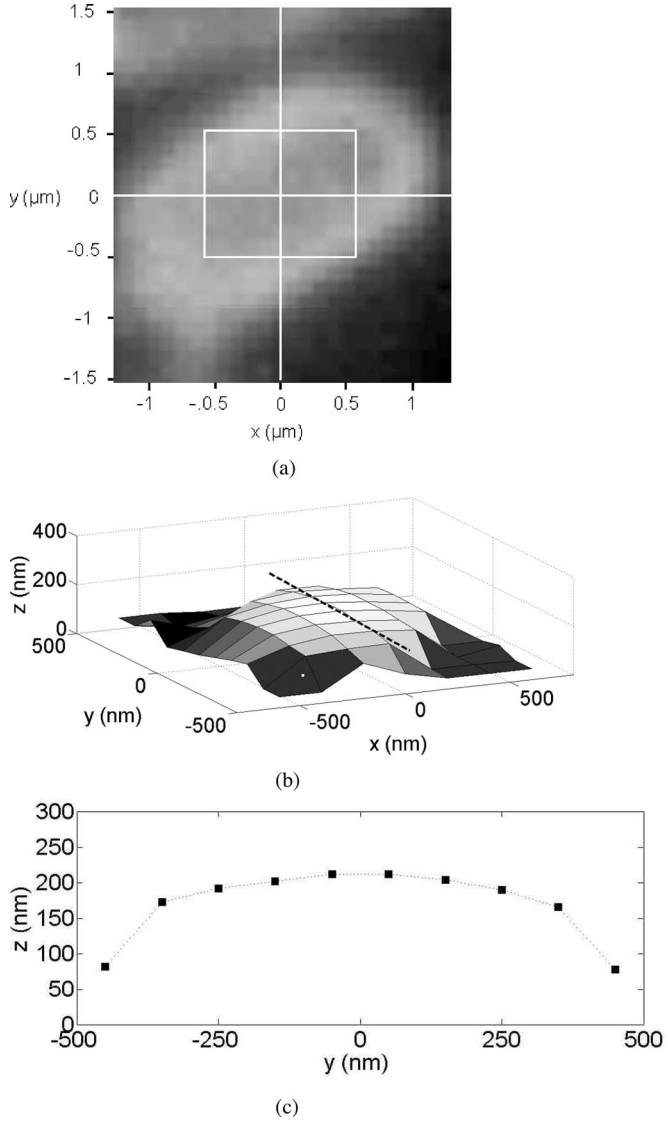

Fig. 10. (a) Wide-field fluorescence image of a *Shigella flexneri* bacterium. Rectangular area probed by 4Pi-SSFM is marked. (b) Surface plot of the bacterial membrane probed by 4Pi-SSFM. (c) Line cut of the surface profile along the dashed line shown in (b).

to probe the surface profile. The fluorophores were dissolved in dimethylsulfoxide (DMSO) and applied to the functionalized surface for half an hour. The surface was then washed three times with methanol, dried with argon, and another cover slip was placed on top with immersion oil in between. Finally, the two cover slips were sealed with nail polish.

For spectral acquisition, the ridge sample was placed in the common focus of the objectives and scanned laterally across the stripes with 500 nm steps. The spectra of the monolayer of fluorophores revealed oscillations with a high visibility of about 0.75. Spectral shifts were observed for different axial positions of the fluorophore monolayer. After the fittings, the 20-nm-etch features were recovered from the raw spectrum, and the axial profile of the ridges along one lateral dimension is plotted in Fig. 9 after the tilt on the sample with respect to the optical axis was corrected. Between the 2 and 7 μm lateral points indicated in Fig. 9(a), the standard deviation of the axial position values was 1.8 nm. Between the 7 and 12 μm points, the profile was smoother and the standard deviation of axial positions in this lateral range was 0.5 nm. Simulations using comparable fringe visibility and SNR predict less than 1 nm of standard deviation. The slightly higher variation here is due to the mechanical vibrations in the system. Furthermore, the uncommon path length for the two collection pathways is at least four orders of magnitude larger than that of the oxide of a flat wafer, and thus, 4Pi-SSFM is more prone to environmental disturbances when compared to the standard reflection mode SSFM. Nonetheless, the microscope is stable enough and can still localize the fluorescent monolayers at the nanometer scale.

We have also used the 4Pi-SSFM system to probe the outer membrane of the gram-negative bacterium *Shigella flexneri*, a rod-shaped human pathogen that is typically 1.5–2 μm in diameter and 4–5 μm in length. The outer membrane of the bacteria was stained by addition of the FM4-64 dye to a concentration of 25 μM in the culture medium for 60 min during exponential phase growth. FM4-64 dye has an absorption maximum of 515 nm and an emission maximum of 640 nm. Although the laser wavelength we use is less than the absorption maximum, the absorption spectrum is sufficiently wide and the dye is excitable using a 488 nm source. The labeled bacteria was harvested by centrifugation and fixed to a poly-L-lysine-coated glass cover slip. The mounting medium [0.1 M N-propyl gallate in 20 mM

Tris–HCl, pH 8.0, 154 mM NaCl, 0.02% NaN_3, 50% (v/v) glycerol] was added to the sample, which was then covered with a second glass cover slip. The outer membrane of the bacterium on the opposite side of the bacterium–glass contact was then probed by recording self-interference spectra. The sample was scanned laterally within about a 1 μm^2 area with 200 nm steps in the x-direction and 100 nm steps in the y-direction to generate a 3-D dataset containing two spatial coordinates and the spectral dimension. The integration time for each spectrum was 10 s that enabled us to collect maximum counts of approximately 1000 in order to ensure nanometer scale localization in the fitting procedure. We modeled the emission to be isotropic although the fluorophores might have a particular dipole orientation in the membrane. In determining the relative axial position of the fluorophores compared to axial position of nearby lateral points, this approach is sufficient and errors are within the uncertainty of the localization. In our application, there is a mismatch between the refractive indexes of the mounting medium and the objective immersion medium. Although it is desirable to match the refractive indexes to minimize any distortions in the point spread function of the microscope, it is not as critical in localization as compared to imaging applications. By analyzing the spectral fringes, we determined the relative axial position of each lateral point. As demonstrated in Fig. 10, we generated a surface plot of the bacterial outer membrane that is a few micrometers away from the coverslip surface. Techniques like FLIC microscopy or reflection interference contrast microscopy (RICM), which are utilized to provide membrane topography, localize membrane-bound fluorophores close to solid supports [25]. On the other hand, 4Pi-SSFM inherently does not rely on the presence of a support to determine the axial position. Thus, using 4Pi-SSFM, it is possible to study subcellular structures away from surfaces to avoid surface related effects.

IV. Conclusion

The SSFM utilizing the reflection from planar surfaces is a very convenient tool for determining the axial position of fluorescent emitters in low-NA applications where lateral resolution is not critical. On the other hand, high-lateral resolution is not possible while maintaining high-axial localization precision. 4Pi-SSFM that is capable of axial localization while employing high-numerical aperture objectives for high-lateral resolution is a promising technique for the analysis of cell surface structures of bacteria. Here, we have performed high-resolution imaging of the membrane of a gram-negative bacterium. In addition to the membrane, the bacterial surface contains multiple biologically important structures, including a protective polysaccharide layer, surface protein receptors, and specialized secretion systems. These surface structures interact with molecules in the environment and, during bacterial infection of mammalian hosts with components of the mammalian cell. The spatial positioning of these molecules is critical to these interactions. 4Pi-SSFM is promising as a tool for the analysis of the positioning of these structures *in vitro* and under biologically relevant conditions.

Acknowledgment

The authors would like to thank S. Ippolito for his help in building the 4Pi-SSFM microscope and B. Davis for discussions on the imaging capabilities of SSFM and 4Pi systems.

References

[1] E. Abbe, "Beitrage zur Theorie des Mikroskops und der mikroskopischen Wahrnehmung," *Arch. Mikrosk. Anat. Entwicklungmech.*, vol. 9, pp. 413–468, 1873.

[2] S. W. Hell and E. H. K. Stelzer, "Properties of a 4Pi confocal fluorescence microscope," *J. Opt. Soc. Amer. A*, vol. 9, pp. 2159–2166, 1992.

[3] S. W. Hell, S. Lindek, C. Cremer, and E. H. K. Stelzer, "Measurement of the 4Pi-confocal point spread function proves 75 nm axial resolution," *Appl. Phys. Lett.*, vol. 64, pp. 1335–1337, 1994.

[4] S. W. Hell and J. Wichmann, "Breaking the diffraction resolution limit by stimulated emission: Stimulated-emission-depletion fluorescence microscopy," *Opt. Lett.*, vol. 19, pp. 780–782, 1994.

[5] T. A. Klar, S. Jakobs, M. Dyba, A. Egner, and S. W. Hell, "Fluorescence microscopy with diffraction resolution barrier broken by stimulated emission," *Proc. Natl. Acad. Sci. USA*, vol. 97, pp. 8206–8210, 2000.

[6] M. G. L. Gustafsson, "Nonlinear structured-illumination microscopy: Wide-field fluorescence imaging with theoretically unlimited resolution," *Proc. Natl. Acad. Sci. USA*, vol. 102, pp. 13081–13086, 2005.

[7] A. Yildiz, J. N. Forkey, S. A. McKinney, T. Ha, Y. E. Goldman, and P. R. Selvin, "Myosin V walks hand-over-hand: Single fluorophore imaging with 1.5-nm localization," *Science*, vol. 300, no. 5628, pp. 2061–2065, 2003.

[8] A. Yildiz, M. Tomishige, R. D. Vale, and P. R. Selvin, "Kinesin walks hand-over-hand," *Science*, vol. 303, no. 5658, pp. 676–678, 2004.

[9] M. J. Rustl, M. Bates, and X. Zhuang, "Sub-diffraction-limit imaging by stochastic optical reconstruction microscopy (STORM)," *Nat. Methods*, vol. 3, pp. 793–796, 2006.

[10] E. Betzig, G. H. Patterson, R. Sougrat, O. W. Lindwasser, S. Olenych, J. S. Bonifacino, M. W. Davidson, J. Lippincott-Schwartz, and H. F. Hess, "Imaging intracellular fluorescent proteins at nanometer resolution," *Science*, vol. 313, pp. 1642–1645, 2006.

[11] O. Wiener, "Stehende Lichtwellen und die Schwingungrichtung polarisirten Lichtes," *Ann. Phys. Chem.*, vol. 40, pp. 203–243, 1890.

[12] K. H. Drexhage, "Influence of a dielectric interface on fluorescence decay time," *J. Lumin.*, vol. 1/2, pp. 693–701, 1970.

[13] W. Lukosz and R. E. Kunz, "Light emission by magnetic and electric dipoles close to a plane dielctric interface. I. Total radiated power," *J. Opt. Soc. Amer.*, vol. 67, no. 12, pp. 1607–1615, 1977.

[14] K. H. Drexhage, "Interaction of light with monomolecular dye layers," *Prog. Opt.*, vol. 12, pp. 163–232, 1974.

[15] A. Lambacher and P. Fromherz, "Fluorescence interference-contrast microscopy on silicon using a monomolecular dye layer," *Appl. Phys. A*, vol. 63, pp. 207–216, 1996.

[16] D. Braun and P. Fromherz, "Fluorescence interference-contrast microscopy of cell adhesion on silicon," *Appl. Phys. A*, vol. 65, pp. 341–348, 1997.

[17] A. Lambacher and P. Fromherz, "Luminescence of dye molecules on oxidized silicon and fluorescence interference contrast microscopy of biomembranes," *J. Opt. Soc. Amer. B*, vol. 19, pp. 1435–1453, 2002.

[18] A. K. Swan, L. Moiseev, C. R. Cantor, B. Davis, S. B. Ippolito, W. C. Karl, B. B. Goldberg, and M. S. Unlu, "Towards nanometer-scale resolution in fluorescence microscopy using spectral self-iterference," *IEEE J. Sel. Topics Quantum Electron.*, vol. 9, no. 2, pp. 294–300, Mar./Apr. 2003.

[19] P. Goy, J. M. Raimond, M. Gross, and S. Haroche, "Observation of cavity-enhanced single-atom spontaneous emission," *Phys. Rev. Lett.*, vol. 50, pp. 1903–1906, 1983.

[20] D. Englund, D. Fattal, E. Waks, G. Solomon, B. Zhang, T. Nakaoka, Y. Arakawa, Y. Yamamoto, and J. Vuckovic, "Controlling the spontaneous emission rate of single quantum dots in a two-dimensional photonic crystal," *Phys. Rev. Lett.*, vol. 95, pp. 013904-1–013904-4, 2005.

[21] H. Schniepp and V. Sandoghdar, "Spontaneous emission of europium ions embedded in dielectric nanospheres," *Phys. Rev. Lett.*, vol. 89, pp. 257403-1–257403-4, 2002.

[22] L. A. Moiseev, A. K. Swan, M. S. Ünlü, B. B. Goldberg, and C. R. Cantor, "DNA conformation on surfaces measured by fluorescence self-interference," *Proc. Natl. Acad. Sci. USA*, vol. 103, pp. 2623–2628, 2006.

[23] L. A. Moiseev, C. R. Cantor, I. Aksun, M. Dogan, B. B. Goldberg, A. K. Swan, and M. S. Ünlü, "Spectral self-interference fluorescence microscopy," *J. Appl. Phys.*, vol. 96, pp. 5311–5315, 2004.
[24] B. J. Davis, M. Dogan, B. B. Goldberg, W. C. Karl, M. S. Ünlü, and A. K. Swan, "4Pi spectral self-interference microscopy," *J. Opt. Soc. Amer. A*, vol. 24, no. 12, pp. 3762–3771, 2007.
[25] R. Parthasarathy and J. T. Groves, "Optical techniques for imaging membrane topography," *Cell Biochem. Biophys.*, vol. 41, pp. 391–413, 2004.

Mehmet Doğan (S'07) was born in Balikesir, Turkey, in 1978. He received the B.S. degree in physics from Bilkent University, Ankara, Turkey, in 2000, and the M.A. degree in physics in 2002 from Boston University, Boston, MA, where he is currently working toward the Ph.D. degree in physics.

His current research interests include modeling of optical systems, high-resolution optical system design, and interferometric fluorescence imaging techniques.

Mr. Doğan has been a member of the American Physical Society, the Optical Society of America, the Materials Research Society, and the IEEE Lasers and Electro-Optics Society.

Ayça Yalçın (S'04) was born in Istanbul, Turkey, in 1982. She received the B.S. degree in electrical and electronics engineering from Bilkent University, Ankara, Turkey, in 2003, and the M.S. degree in photonics in 2005 from Boston University, Boston, MA, where she is currently working toward the Ph.D. degree in electrical and computer engineering.

Her current research interests include optical microresonator biosensors and interferometric techniques in fluorescence microscopy.

Ms. Yalçın is a member of the American Physical Society and the IEEE Lasers and Electro-Optics Society.

Sumita Jain was born in Bangalore, India, in 1972. She received the B.Sc. degree from Mount Carmel College, Bangalore, India, and the Ph.D. degree in microbiology from the University of Tennessee Health Science Center, Memphis, TN, in 2000.

She was a Postdoctoral Researcher in bacterial pathogenesis at Harvard Medical School and Massachusetts General Hospital, Boston. She is currently a Senior Fellow at the University of Washington, Seattle. Her current research interests include the molecular mechanisms of bacterial pathogenesis and host-pathogen interactions.

Marcia B. Goldberg was born in Boston, MA, in 1957. She received the B.A. degree from Harvard University, Cambridge, MA, in 1979, and the M.D. degree from Harvard Medical School, Boston, in 1984.

She was a Postdoctoral Researcher in microbial pathogenesis at Massachusetts General Hospital, Boston, and at the Pasteur Institute, Paris, France. In 1993, she joined the Microbiology and Immunology Faculty of Albert Einstein College of Medicine, Yeshiva, University, New York, and in 1999, she joined the Infectious Diseases and Microbiology Faculty of Harvard Medical School, where she is currently an Associate Professor of Medicine (microbiology and molecular genetics). Her current research interests include protein localization in bacteria and molecular mechanisms of host–pathogen interactions.

Anna K. Swan (M'05–SM'07) received the M.S. degree in physics engineering from Chalmers University, Gothenburg, Sweden, in 1986, and the Ph.D. degree in physics from Boston University, Boston, MA, in 1994.

She was with the Solid State Division, Oak Ridge National Laboratory, Oak Ridge, TN, as a Wigner Fellow. She is currently an Associate Professor in the Electrical and Computer Engineering Department, Boston University, with a joint appointment in the Physics Department. Her current research interests include optical studies of 0-D, 1-D, and 2-D systems such as quantum dots, individual carbon nanotubes and graphene, and the topic of this paper, interferometric fluorescence techniques.

Dr. Swan is a member of the American Physical Society and the Optical Society of America. She is the recipient of the Nottingham Prize and the Morton M. Traum Award for her dissertation on spin-ordering on NiO (1 0 0) surfaces using metastable He^* scattering.

M. Selim Ünlü (M'90–SM'95–F'07) received the B.S. degree from the Middle East Technical University, Ankara, Turkey, in 1986, and the M.S.E.E. and Ph.D. degree from the University of Illinois, Urbana-Champaign, in 1988 and 1992, respectively, all in electrical engineering.

In 1992, he joined the Department of Electrical and Computer Engineering, Boston University, Boston, MA, where he is currently a Professor of electrical and computer engineering, biomedical engineering, and physics. He is also serving as an Associate Dean for research and graduate programs in engineering as well as the Associate Director of the Center for Nanoscience and Nanobiotechnology. His current research interests include nanophotonics and biophotonics and research and development of photonic materials, semiconductor optoelectronic devices, high-resolution microscopy and spectroscopy of semiconductor and biological materials, and biological sensing and imaging.

Dr. Ünlü was the Chair of the IEEE Laser and Electro-Optics Society (LEOS), Boston Chapter, from 1994 to 1995, winning the LEOS Chapter-of-the-Year Award. He was the recipient of the National Science Foundation Research Initiation Award in 1993, the United Nations Transfer of Knowledge Through Expatriate Nationals (TOKTEN) Awards in 1995 and 1996, and both the National Science Foundation CAREER and the Office of Naval Research Young Investigator Awards in 1996. He has been a former Chair of the IEEE/LEOS Technical Committee on photodetectors and imaging, and is currently the Chair of the IEEE/LEOS Nanophotonics Committee. He is an Associate Editor for the IEEE JOURNAL OF QUANTUM ELECTRONICS and the Vice President of the LEOS for Membership and Regional Activities—Americas. He has been selected as a LEOS Distinguished Lecturer for 2005–2007 and Australian Research Council Nanotechnology Network (ARCNN) Distinguished Lecturer for 2007.

Bennett B. Goldberg was born in Boston, MA, in 1959. He received the B.A. degree from Harvard College, Cambridge, MA, in 1982, and the M.S. and Ph.D. degrees in physics from Brown University, Providence, RI, in 1984 and 1987, respectively.

He was a Bantrell Postdoctoral Fellow at the Massachusetts Institute of Technology and the Francis Bitter National Magnet Laboratory. In 1989, he joined the Physics Faculty at Boston University, Boston, where he is currently a Professor of physics, electrical and computer engineering, and biomedical engineering. He is also the Chair of the Physics Department. He has worked in near-field imaging of photonic bandgap, ring microcavity, and single-mode waveguide devices, and has recently developed subsurface solid immersion microscopy for Si inspection. He is also the Director of Boston University's new Center for Nanoscience and Nanobiotechnology. His current research interests include ultrahigh-resolution microscopy and spectroscopy techniques for hard and soft material systems.

Prof. Goldberg has been a member of the American Physical Society, the Materials Research Society (MRS), and the IEEE Lasers and Electro-Optics Society.